Journal Name

Dynamic Article Links ►

Cite this: DOI: 10.1039/c0xx00000x

www.rsc.org/xxxxxx

ARTICLE TYPE

Development and performance of $MgFeCrO_4$ – based electrodes for solid oxide fuel cells

Elena Stefan,*[a] Paul A. Connor[a] and John T.S. Irvine*[a]

Received (in XXX, XXX) Xth XXXXXXXXX 20XX, Accepted Xth XXXXXXXXX 20XX

DOI: 10.1039/b000000x

Abstract

Composite anodes for solid oxide fuel cells (SOFC) developed on yttria stabilised zirconia (YSZ) porous supports by infiltration of electrode materials has been successfully applied for various anode and cathode compositions, resulting in high performance SOFC devices. The focus of this study is the performance of the chromium-rich spinel ($MgFeCrO_4$) as an electrode support material when used alone or impregnated. The composite anodes were prepared by aqueous infiltration of nitrate salts to produce $(La_{0.75}Sr_{0.25})_{0.97}Cr_{0.5}Mn_{0.5}O_{3-\delta}$, $Ce_{0.9}Gd_{0.1}O_{2-\delta}$, CeO_2 or Pd into a $MgFeCrO_4$ scaffold with 45% porosity and studied by electrochemical impedance spectroscopy in symmetrical cell configuration. The performance was evaluated in humidified 5%H_2/Ar in order to quantify their stability and performance up to 850 C with respect to the $MgFeCrO_4$ porous substrate. It was found that all the impregnated phases adhere very well to the spinel and considerably enhance performance and stability to a level required for SOFC applications. $MgFeCrO_4$/LSCM/CGO and $MgFeCrO_4$/LSCM/CGO/Pd showed the most substantial improvement in comparison to the scaffolds performance, with ASR values of 1.74 Ωcm^2 and 0.91Ωcm^2, respectively.

1. Introduction

SOFCs are electrochemical devices which convert chemical energy stored in a fuel into electricity, via an electrochemical reaction at elevated temperatures (600-1000 °C).[1,2] The development of fuel cell technology is encouraged by the clean production of electricity from a variety of fuels without the combustion step resulting in higher conversion efficiency and with low emissions of pollutants.[3–6] However, for superior electrochemical performance, the material requirements for such devices are rather demanding and lead to expensive materials. The material requirements along with the tendency of decreasing the functioning temperatures for SOFCs encourage the development of new materials.

Thus, the application of ferritic stainless steels as interconnect materials in SOFCs is a desirable option for decreasing materials costs. These steels have several disadvantages when used in fuel cells, mainly chromium poisoning of electrodes and high temperature oxidation to form oxide scales such as chromia and $(Mn,Fe,Cr)_3O_4$ or $(Mn,Cr)_3O_4$ spinels.[7–12] . The compatibility of the interconnect with the electrode material is directly connected to their interface, where usually the materials may react, leading to performance degradation. Employing chromium-spinels at the interconnect/electrode interface might improve the compatibility as a transition layer between the metal and the electrode oxide materials. The interface interconnect/electrode is poorly optimised in a stack (optimisation of physical and chemical nature), leading to much lower performance of the stacked fuel cells than individually tested cells.[16] The use as a support material of a low cost, redox stable oxide that is compatible with high temperature steels, various electrode materials and YSZ would be of significant value.

We previously reported that several chromium-rich spinels displayed promising chemical stability and electrical conductivity in reducing conditions,[17] leading us to investigate $MgFeCrO_4$ as an anode support material. Spinel $MgFeCrO_4$ has a chemical composition and crystal structure closely related to the oxide scale formed on interconnect surfaces following oxidation of ferritic steels (FeCr alloy). However these materials would not be expected to be good electrodes, without the addition of extra materials to form composite electrodes. LSCM has been previously studied and reported as an efficient stable electrode material in reducing and oxidizing conditions and enhances the electronic conductivity in composite anodes.[18–21] Ionic conductivity is another desirable property for electrode materials, or composite electrodes so ionic conducting materials as CGO or CeO_2 [22] can be added to improve the total performance of the cells. Pd is a well known catalyst to promote electrochemical reactions.[23]

Therefore the aims of this study were to fabricate $MgFeCrO_4$ scaffolds and to evaluate the electrochemical performance of symmetrical cells based on such scaffold impregnated with electrode materials $(La_{0.75}Sr_{0.25})_{0.97}Cr_{0.5}Mn_{0.5}O_{3-\delta}$ (LSCM), $Ce_{0.9}Gd_{0.1}O_{2-\delta}$ (CGO), CeO_2 or Pd.

2. Experimental

Symmetrical cells were produced by tape casting the $MgFeCrO_4$ electrode material with the YSZ electrolyte layer screen-printed on the green (un-sintered) tapes. The final structures were obtained by laminating two green $MgFeCrO_4$/YSZ tapes. Green $MgFeCrO_4$ ceramic tapes were obtained by tape casting a slurry containing spinel powder, organic binder (poly(vinyl-butyrate)), dispersant (dibutyl(phthalate)), plasticiser (poly(ethylene-glycol)) and graphite pore former (~6 wt.% - of total solids). $MgFeCrO_4$ was obtained by combustion synthesis and the experimental description is covered in our previous work.[17] Laminated green tapes were sintered at 1400 °C for 12 h. In the final ceramic structure the 25 µm thick dense electrolyte was enclosed between two porous spinel layers with 45% porosity and 200 µm thickness. The relative density of the sintered scaffold was determined from the measured diameter and thickness (from SEM micrograph), with the electrolyte weight, as estimated from sintering studies of different structures, subtracted from that of the sintered body.

The porous layers were used as scaffolds for LSCM, with additions of CGO, CeO_2 and Pd, which were impregnated into the supports as nitrate solutions prepared with the reagents: $La(NO_3)_3{\cdot}6H_2O$ Alfa Aesar (>99.99%), $Sr(NO_3)_2$ Sigma Aldrich (>99%), $Cr(NO_3)_3{\cdot}9H_2O$ Sigma Aldrich (99.5%), $Mn(NO_3)_2{\cdot}4H_2O$ Alfa Aesar (99.98%), $Ce(NO_3)_3{\cdot}6H_2O$ Aldrich (99%), $Gd(NO_3)_3{\cdot}6H_2O$ Aldrich (99.9%). The desired loadings of electrode and catalyst material were obtained with the impregnation carried out as a multistep process, with intermediary calcinations steps at 500°C and final sintering steps at 1200 °C (4 h) for LSCM, 1000 °C (4 h) for CGO and 450 °C (1 h) for CeO_2 and Pd. The electrodes prepared in this study, with the specific component loadings, in wt. % are labelled as presented in Table 1.

Table 1.Composite electrodes prepared in this study by impregnating porous $MgFeCrO_4$ scaffolds and the nomenclature used for them throughout this paper.

Composition (wt. %)	Label
Support ($MgFeCrO_4$)	$MgFeCrO_4$
+ LSCM (31%)	$MgFeCrO_4$/LSCM
+ LSCM (27%) / CGO (15%)	$MgFeCrO_4$/LSCM/CGO
+ LSCM (27%) / CeO_2 (6%)	$MgFeCrO_4$/LSCM/CeO_2
+ LSCM (27%) / CGO (15%) / Pd(1%)	$MgFeCrO_4$/LSCM/CGO/Pd
+ LSCM (27%) / CeO_2 (6%) / Pd (1%)	$MgFeCrO_4$/LSCM/CeO_2/Pd

$MgFeCrO_4$/LSCM/CGO and $MgFeCrO_4$/LSCM/CeO_2 were prepared by sequential impregnation of materials in order of decreasing required sintering temperature. The formation of perovskite phase inside the scaffolds was confirmed by X-ray diffraction.

Phase analysis for symmetrical cells was performed on a PANalytical Empyrean Diffractometer in reflection mode, while microstructure was observed on a JEOL JSM-6700F Scanning Electron Microscope (SEM).

Electrochemical performance was determined by electrochemical impedance spectroscopy (EIS) in the frequency range of 1 MHz-0.1 Hz with 20 mV AC perturbation amplitude using a Solartron 1260 frequency response analyser and SMaRT v2.8.0 (Solartron Analytical) and ZView v3.1c software (Scribner Associates). The geometric area of symmetrical cell electrodes was 1.2 cm^2 on either side of the dense electrolyte layer. Measurements were made in a single chamber, consisting of a quartz tube with one open end in which a two electrode alumina testing jig was inserted and closed gas tight. The alumina jig had inlet and outlet for gas flow (humidified (3%H_2O) 5%H_2/Ar) and platinum wires for electrical contact to the sample and a sample thermocouple. Measurements included temperature dependence and assessment of the reduction process at a constant temperature of 850 °C. The ohmic resistance of the testing jig and constituent Pt wires was measured and subtracted from the results obtained for symmetrical cells. In order to remove the contribution of the thin YSZ electrolyte layer in the series resistance (R_s), a pellet of YSZ was measured by AC impedance and the resistance of the electrolyte layer was calculated and subtracted from the R_s value.

3. Results and discussion

3.1 Phase analysis and microstructure of $MgFeCrO_4$ scaffold

The requirements for the application of $MgFeCrO_4$ as electrode support on the fuel side of SOFCs comprise chemical and microstructural stability of the spinel under reducing conditions. We assessed the chemical stability of $MgFeCrO_4$ in dry and humidified 5%H_2/Ar at 1000 °C for 20 h. When reduced in dry 5%H_2/Ar, the $MgFeCrO_4$ decomposed, with segregation of metallic Fe and MgO The material reduced in humidified 5%H_2/Ar did not decompose, as the partial pressure of oxygen (p_{O_2}) was above the stability limit for which secondary phases did not segregate from the spinel (Fig. 1). When reduced at 850 °C for 30 h in dry 5%H_2/Ar the $MgFeCrO_4$ showed no sign of decomposition, which indicates stability in fuel environments when operated lower than 850 °C.

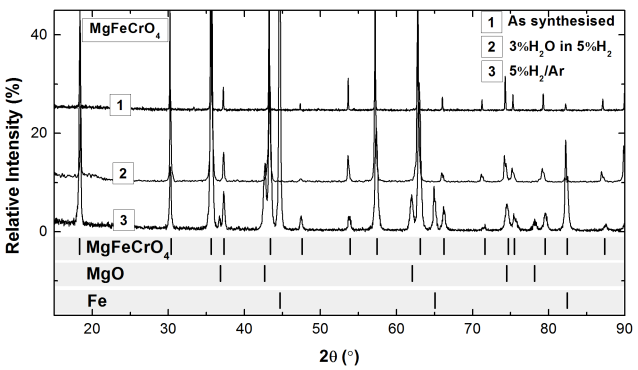

Fig. 1 X-ray diffraction pattern of $MgFeCrO_4$ scaffold reduced in dry 5%H_2/Ar or humidified 5%H_2/Ar at 1000 °C for 20 h.

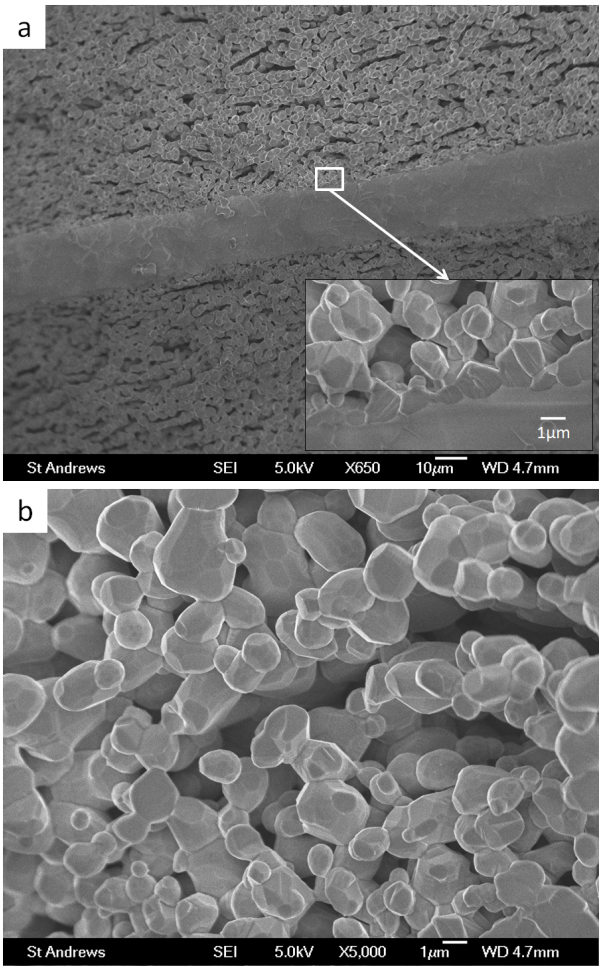

Fig. 2 Micrograph of $MgFeCrO_4$ / YSZ / $MgFeCrO_4$ scaffold, with detail of the spinel/YSZ interface and the spinel porous layer.

In Fig. 2 are illustrated SEM images in cross-section of the $MgFeCrO_4$ scaffold, with a general overview of the symmetrical architecture, the thickness of the YSZ electrolyte and the interface formed between YSZ and spinel. Sintered ceramic bodies were not cracked or curved after sintering, thus affirming that any difference in thermal expansion coefficient is small enough to not cause any significant mechanical damage. The spinel had particle size 1-5 μm, good connectivity and open porosity for loading other materials by impregnation.

3.2 DC conductivity of $MgFeCrO_4$ scaffold

DC conductivity was measured at 850°C on a 63% dense pellet switching from static air to humidified 5%H_2/Ar (log p_{O_2} ~ -18). The conductivity increased significantly from 0.014 Scm^{-1} to 0.36 Scm^{-1} upon this reduction, indicating the n-type behaviour for the material, as illustrated in Fig. 3.

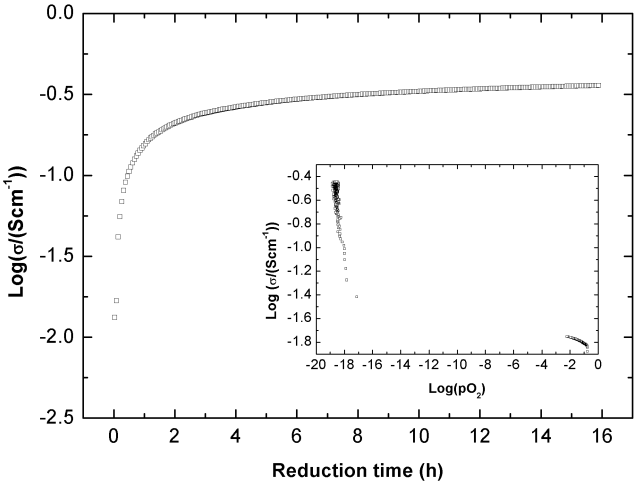

Fig. 3. DC electrical conductivity of a 63% dense $MgFeCrO_4$ pellet plotted as a function of time in reducing conditions at 850 °C. The inner plot shows the same data as a function of p_{O_2}.

3.3 Phase analysis and microstructure of impregnated $MgFeCrO_4$ scaffolds

XRD patterns corresponding to $MgFeCrO_4$/LSCM and $MgFeCrO_4$/LSCM/CGO are presented in Fig. 4 and the patterns for $MgFeCrO_4$/LSCM/CeO_2 in Fig. 5. All the peaks observed in the XRD patterns correspond to phases present in the samples: spinel and perovskite or spinel, perovskite and CGO, or CeO_2 respectively. The XRD pattern for $MgFeCrO_4$/LSCM/CeO_2 (Fig. 5) showed broad peaks corresponding to CeO_2 which is an indication that the Cerium nitrate has decomposed with the formation of CeO_2 with very small particle size.

In Fig. 6 cross-sectional SEM images from samples tested in humidified 5%H_2/Ar are presented. Cross-sectional SEM images confirm that infiltrated phases have good adherence and coverage to the scaffold, while images from the surface show mostly the microstructure of the infiltrated phases. In Fig. 6a, the micrograph for $MgFeCrO_4$/LSCM showed LSCM particles (500 nm – 1 μm) that adhere well to the spinel particles. $MgFeCrO_4$/LSCM/CeO_2 (Fig. **6**b) had a microstructure similar to $MgFeCrO_4$/LSCM samples and ceria nano-particles could be observed. The micrograph of $MgFeCrO_4$/LSCM/CGO (Fig. 6c) confirmed that additional thermal treatments at 1000 °C following the infiltration of CGO, led to densification of LSCM layer, while CGO particles of size 0.1-0.5 μm were apparently very well connected to the LSCM layer. For $MgFeCrO_4$/LSCM/CeO_2/Pd sample, CeO_2 and the assumed to be Pd nano-particles could be observed on the LSCM layer. In Fig. 6e,f is illustrated the microstructure of $MgFeCrO_4$/LSCM/CGO/Pd in cross section (e) and surface (f) suggesting the presence of Pd nanoparticles with size ~10-20 nm on top of larger particles of CGO. Pd nanoparticles are expected to behave as electrocatalytic sites during symmetrical cell electrochemical testing.

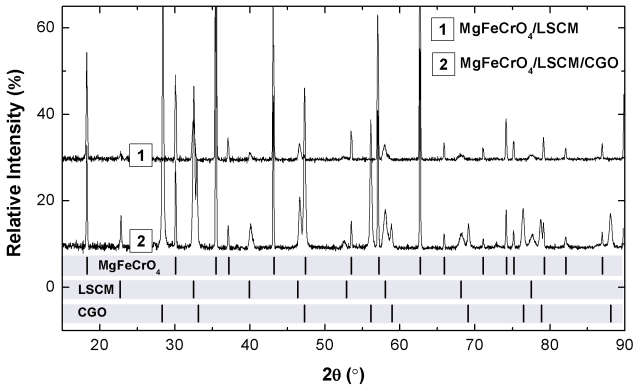

Fig. 4 X-ray diffraction pattern of $MgFeCrO_4$/LSCM and $MgFeCrO_4$/LSCM/CGO with LSCM sintered at 1200 °C (4 h) and CGO at 1000 °C (4 h).

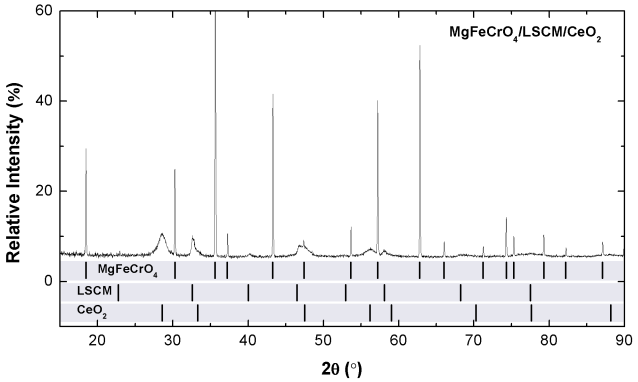

Fig. 5 X-ray diffraction pattern of $MgFeCrO_4$/LSCM/CeO_2 with LSCM sintered at 1200 °C (4 h) and CeO_2 at 450 °C (4 h).

Cite this: DOI: 10.1039/c0xx00000x

www.rsc.org/xxxxxx

ARTICLE TYPE

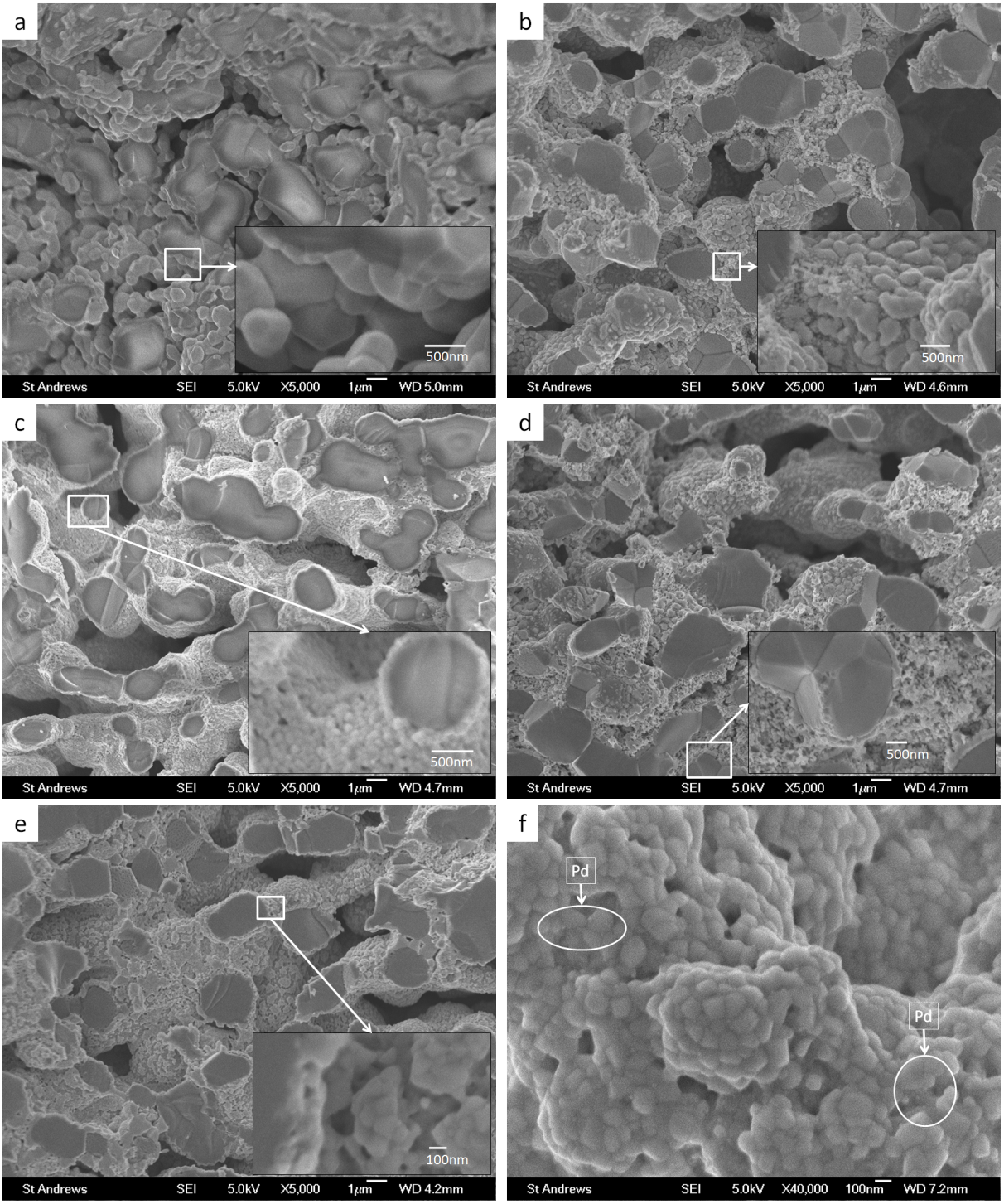

Fig. 6 SEM images in cross-section of: (a) $MgFeCrO_4$/LSCM; (b) $MgFeCrO_4$/LSCM/CeO_2; (c) $MgFeCrO_4$/LSCM/CGO; (d) $MgFeCrO_4$/LSCM/CeO_2/Pd; (e) $MgFeCrO_4$/LSCM/CGO/Pd; (f) surface micrograph for $MgFeCrO_4$/LSCM/CGO/Pd - Pd particles . The micrographs were collected after the samples were tested in humidified 5%H_2/Ar.

Cite this: DOI: 10.1039/c0xx00000x

www.rsc.org/xxxxxx

ARTICLE TYPE

3.4 Electrochemical performance of impregnated $MgfeCrO_4$ scaffolds

The electrochemical performance of the impregnated scaffolds measured in 5%H_2/Ar suggests their suitability as SOFC anodes, for realistic, fully humidified fuels. Comparative impedance spectra for the symmetrical cells at 850 °C in humidified 5%H_2/Ar are displayed as Nyquist and Bode plots in Fig. 7a,b. Results obtained by fitting the experimental data to the equivalent circuit illustrated in Fig. 8, are summarised in Table 2. The temperature dependence of ohmic resistances (R_s) and polarisation resistances (R_p) values are shown in Fig. 7c,d as Arrhenius plots. The ohmic resistance of the scaffold had a significantly lower value (R_s=0.47 Ωcm^2), in comparison with the other impregnated samples (Table 2). The R_s value increased with the infiltration of various phases, and the most for $MgFeCrO_4$/LSCM. Even after reduction the R_s value of $MgFeCrO_4$/LSCM remained the highest amongst the tested samples, 4.65 Ωcm^2. This may have been caused by two different contributions: first, the efficient reduction of the $MgFeCrO_4$ scaffold was observed to have a major impact for the ohmic resistance, thus when infiltrated into the non-reduced scaffold, LSCM had a good adherence to the spinel particles and hindered the efficient reduction of the scaffold. Secondly, LSCM has p-type conductivity and in reducing atmosphere, its electronic conductivity decreases,[18,24] thus its contribution led to an increase of the the ohmic resistance. However, the infiltration of LSCM into the scaffold had a positive effect for the R_p value, as its electrochemical properties are superior to the spinel. The addition of CeO_2 or CGO further improved the cell performances, with both R_s and R_p decreasing. R_s values for $MgFeCrO_4$/LSCM/CGO and $MgFeCrO_4$/LSCM/CeO_2 were about the same, while R_p values seemed to decrease in proportion to the quantity of ionic conducting material impregnated into the sample. $MgFeCrO_4$/LSCM/CGO/Pd and $MgFeCrO_4$/LSCM/CeO_2/Pd showed even better performance in R_s and R_p, as presented in Fig. 7a. Thus, the addition of catalysts contributed positively to the electrochemical tests, presumably by facilitating surface exchange reaction which is the initial step in the reduction of the scaffold. The reduced surface layer resulted in formation of a conduction path with increased conductivity.

Cite this: DOI: 10.1039/c0xx00000x

www.rsc.org/xxxxxx

ARTICLE TYPE

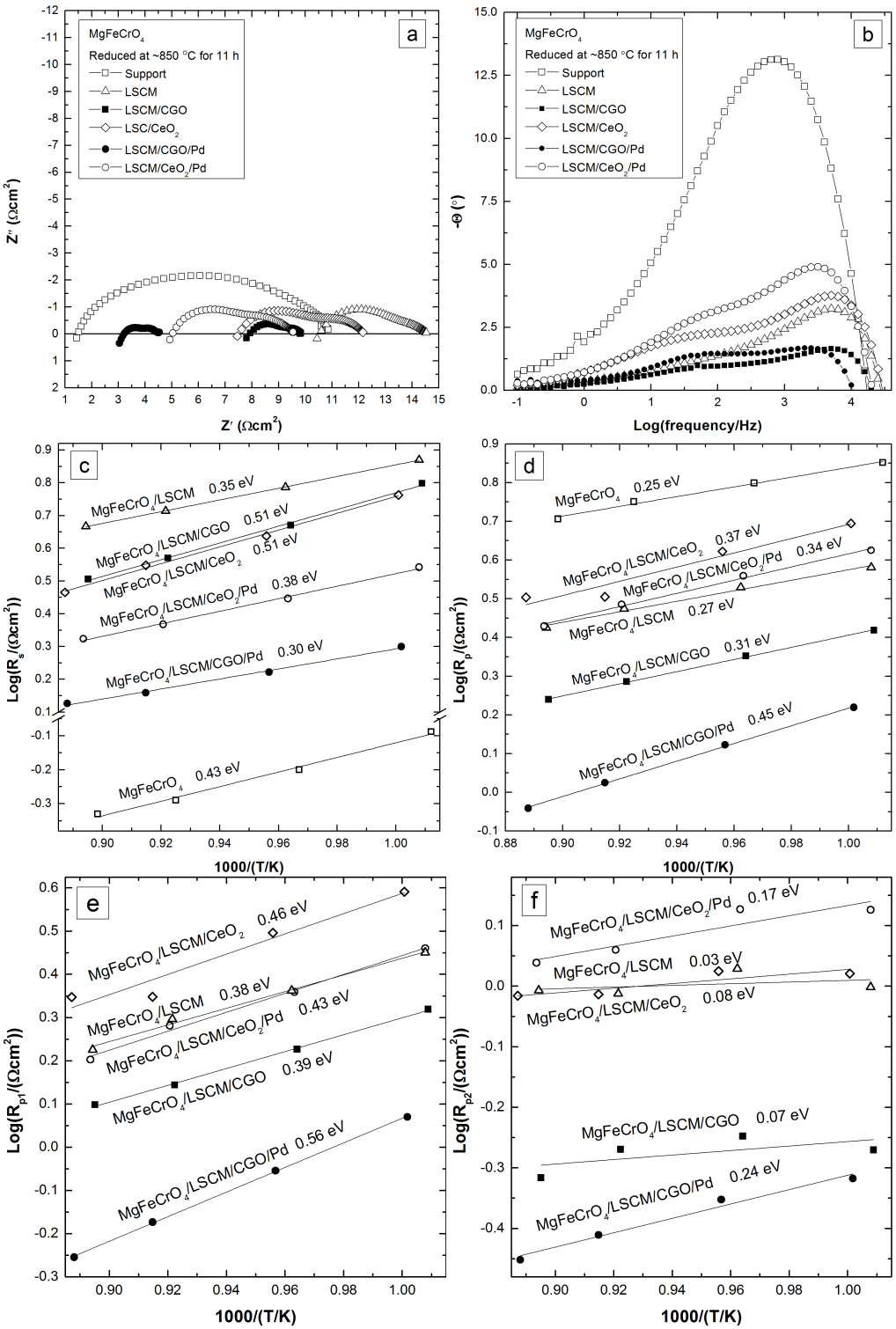

Fig. 7 Symmetrical cells measured in humidified 5%H_2/Ar at 850 °C: (a) Nyquist plot containing data for the whole cell (two equal electrodes); (b) Bode plot of phase angle vs. frequency; (c), (d), (e), (f) Arrhenius plots for R_s, R_p R_{p1} and R_{p2} resulted from equivalent circuit fitting of experimental data. The plotted R_s and R_p values are for one electrode are corrected for jig and electrolyte resistance.

Cite this: DOI: 10.1039/c0xx00000x

www.rsc.org/xxxxxx

ARTICLE TYPE

Table 2. Relaxation frequencies and polarisation resistances for symmetrical cells tested in humidified 5%H_2/Ar at ~850 °C. R_s and R_p (R_{p1}, R_{p2}) are determined from equivalent circuits fitting and listed values are for one electrode.

Electrode	R_s (Ωcm^2)	R_p (Ωcm^2)	f_{max1} (Hz)	Process 1	f_{max2} (Hz)	Process 2	R_{p1} (Ωcm^2)	R_{p2} (Ωcm^2)
$MgFeCrO_4$	0.47	5.09	1200	Charge transfer	132	Dissociative gas adsorption	0.80	4.29
$MgFeCrO_4$/LSCM	4.65	2.66	5250	Charge transfer	190	Dissociative gas adsorption	1.68	0.98
$MgFeCrO_4$/LSCM/CGO	3.20	1.74	6310	Charge transfer	76	Dissociative gas adsorption	1.25	0.48
$MgFeCrO_4$/LSCM/CeO_2	2.92	3.19	5250	Charge transfer	30	Dissociative gas adsorption	2.23	0.96
$MgFeCrO_4$/LSCM/CGO/Pd	1.33	0.91	3020	Charge transfer	63	Dissociative gas adsorption	0.56	0.35
$MgFeCrO_4$/LSCM/CeO_2/Pd	2.10	2.68	3630	Charge transfer	63	Dissociative gas adsorption	1.60	1.10

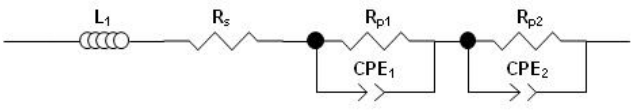

Fig. 8 Equivalent circuit used to fit experimental data, where L=inductor; R_s=series resistance; R_p=polarisation resistance and CPE=constant phase element.

Impedance spectra showed two arcs, one process distinguishable at high frequency and one process at low frequency. The presence of two semicircles was observable for all the impregnated samples, while the scaffold showed a single bigger and depressed arc. The high frequency arc was always the largest and both processes were changing for different catalysts infiltrated into scaffolds. The attribution of processes is based on relaxation frequency,[25–27] which in this study were determined from equivalent circuits fitted to Bode plots (-Z"vs.f). The high frequency process corresponds to charge transfer and the low frequency process could be attributed to gas adsorption/desorption or association/dissociation. $MgFeCrO_4$ is not expected to be an ionic conductor, thus the high frequency process with f_{max1}=1200 Hz corresponds to electronic transfer, while the low frequency process with f_{max2}=132 Hz, is most likely gas adsorption/desorption. Relaxation frequencies determined for $MgFeCrO_4$/LSCM had similar magnitudes to the scaffold ones, 5250 Hz for high frequency process and 190 Hz at low frequency, corresponding probably to the same processes as previously described, charge transfer, at high frequency and gas adsorption/desorption, at low frequency. Table 2 summarizes relaxation frequencies, the associated processes at high and low frequency and R_{p1} and R_{p2} values corresponding to each process. Scaffolds infiltrated with different materials showed the same trend, the resistance was higher for charge transfer than for gas adsorption/desorption and association/dissociation, while the uninfiltrated scaffold showed higher resistance for gas kinetic processes than for charge transfer. Activation energies (E_a) for R_s and R_p are included in Fig. 7c,d, where E_a for R_s is related to the conduction activation and E_a for R_p is related to the electrochemical processes described by the impedance spectra in Fig. 7a. The E_a with regard to R_s (0.35 eV) for $MgFeCrO_4$/LSCM was smaller than E_a value of 0.56 eV measured for LSCM in 5%H_2/Ar[18] and the E_a value 0.43 eV determined for the scaffold. E_a values for R_s generally remained below 0.51 eV, value that corresponded to $MgFeCrO_4$/LSCM/CGO and $MgFeCrO_4$/LSCM/CeO_2. In air, the reported E_a values for CGO are 0.60 eV[28] and 0.64 eV[29], for which the conductivity is mostly ionic. However, in reducing conditions mixed ionic-electronic conductivity may arise due to the reduction of Ce^{4+} to Ce^{3+}. The conductivity mechanism for the electrons is considered to be small polaron activated hopping process which implies low mobility.[29] These contributions explain to certain extent, the increase in E_a with CGO and CeO_2 infiltration. The E_a values for R_p showed an increase from the scaffold (0.25 eV) to the composite electrodes, with a maximum value of 0.45 eV observed for $MgFeCrO_4$/LSCM/CGO/Pd. As illustrated in Fig. 7e,f, the activation energies for R_{p1} and R_{p2} components of the R_p values indicate that the charge transfer process is more temperature dependent and has a larger resistance than the gas adsorption process.

The best achieved electrochemical performance was for $MgFeCrO_4$/LSCM/CGO/Pd, which was comparable to results reported for LSCM used as an SOFC anode material. In humidified 5%H_2/Ar at 850°C, R_p of 0.59 Ωcm^2 has been observed,[18,20] while at 900 °C R_p values of 0.51 Ωcm^2 (ref [18]) and 0.43 Ωcm^2 (ref [20]) have been measured. In humidified H_2 at 900 °C, D.M Bastidas et al[19] reported an R_p of 0.3 Ωcm^2, while S.P. Jiang et al[30] reported R_p values for a 1:1 composite LSCM-YSZ, with LSCM obtained by gel-casting or solid state reaction of 1.1 Ωcm^2 and 1.9 Ωcm^2, respectively. The comparable results obtained here relative to results reported in the literature are encouraging since the $MgFeCrO_4$ scaffold is not ionically conducting and since the amount of loaded perovskite was limited. Furthermore, E_a values for R_p included in Fig. 7d were lower than E_a values of between 0.70-0.90 eV reported by S.P. Jiang et al[30] for LSCM/YSZ composite anodes.

3.5 Influence of prolonged reduction of impregnated $MgFeCrO_4$ scaffold upon electrochemical performance

The electrochemical performance of the symmetrical cells after prolonged exposure to humidified 5%H_2/Ar is relevant for evaluating the stability of the tested SOFC anodes. The reduction process was performed on symmetrical cells heated to ~850 °C in humidified 5%H_2/Ar. Once constant temperature was reached, impedance measurements were taken after 1 h and 11 h. Nyquist plots for measurements after 1 h and 11 h are compared in Fig. 9a-f, to estimate the influence of reduction upon tested scaffolds infiltrated with different catalysts.

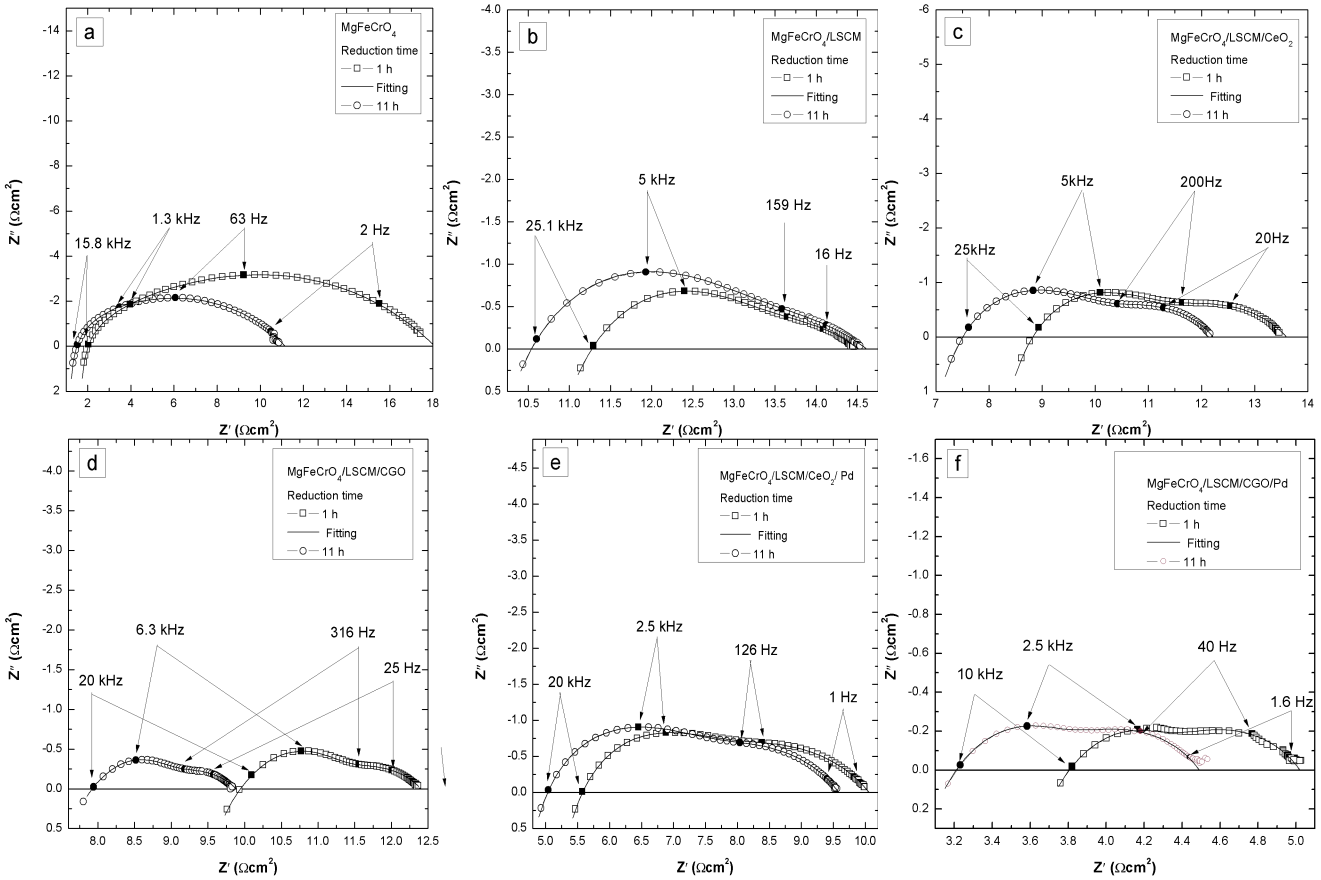

Fig. 9 Nyquist plots for the samples reduced at 850 °C for 1 h/11 h and the corresponding equivalent circuit fit; spectra contain data for 2 identical electrodes.

The performance of the cells improved with increasing reducing time consistently: for $MgFeCrO_4$ the reduction had a significant contribution in decreasing the R_p value (3.26 Ωcm^2), decrease in resistance that corresponded to the low frequency process, possibly due to improvements in the gas surface exchange kinetics after reduction. $MgFeCrO_4$/LSCM showed a decrease in R_s and an increase in R_p corresponding to an increase in resistance of both high and low frequency processes: 0.12 Ωcm^2 for R_{p1} and 0.21 Ωcm^2 for R_{p2}. $MgFeCrO_4$/LSCM/CeO_2 had a small decrease of R_p and an important decrease of R_s of about 0.55 Ωcm^2 after 11 h of reduction. Reduction of $MgFeCrO_4$/LSCM/CGO showed a significant improvement in R_s (~1 Ωcm^2 decrease) and R_p (~0.22 Ωcm^2 decrease in R_{p1} and ~0.08 Ωcm^2 decrease in R_{p2}). $MgFeCrO_4$/LSCM/CeO_2/Pd and $MgFeCrO_4$/LSCM/CGO/Pd had similar improvement in the cells performance after reduction with a decrease of R_s values (~0.3 Ωcm^2), while R_p did not change. The values reported above are for one electrode. The reduction in R_s and R_p could be attributed mostly to the reduction of the support material. Only $MgFeCrO_4$/LSCM showed an increase in R_p that could be explained by the p-type semiconductor behaviour of the LSCM, with the reduction of its conductivity in 5%H_2/Ar.[31] The reduction process had positive effects for cell performance and this contribution was more important than the negative effect corresponding to sintering of ceria nano-particles,[32] a process that cannot be noticed here.

The modelled data are in a good agreement with the measured points indicating a good fit of the equivalent circuit with the electrochemical processes identified for the samples.

4. Conclusions

Porous scaffolds of $MgFeCrO_4$ were prepared in symmetrical configuration by combining tape casting and screen printing techniques. $MgFeCrO_4$ was stable when reduced in dry 5%H_2/Ar, at 850 °C and in humidified 5%H_2/Ar, at 1000 °C. Thus, the material could be applied as support material in a number of other high temperature devices that do not need to operate at extreme very low p_{O_2} values (e.g. electrolysers – steam or CO_2, ammonia

fuel cells, direct carbon fuel cells etc.)

In terms of chemical stability, the results presented above suggest that there is no or limited reactivity between $MgFeCrO_4$ and other cell materials. $MgFeCrO_4$ had satisfactory performance as anode electrode support, as the infiltrated materials had a good adherence to the spinel particles. The formed coating diminished the scaffolds reduction, thus leading to an increase in R_s for tested samples. However, the insertion of electrode materials into the scaffolds decreased polarisation resistances of the cells, as it formed a new conducting path and their electrochemical activity was superior to the spinel. Further catalyst insertion facilitated the reduction of the scaffold and, as expected, enhanced the performance of symmetrical cell as new electrocatalytic sites were active during electrochemical tests. The reduction process had a positive influence for the symmetrical cells performance even if hindered by infiltrated electrode materials. Overall, both reduction process and increase of electrocatalytic activity determined improvements in the electrochemical performance.

Acknowledgements

The authors thank the Office of Naval Research, USA, grant code N00014-11-1-0247, the Engineering and Physical Sciences Research Council, UK, grant platform EP/E064248/1 and the European Union's Seventh Framework Programme (FP7/2007-2013) for the Fuel Cell and Hydrogen Joint Technology initiative under grant agreement n°[FCH JU-GA 278257]10 for financial support.

Notes and references

[a] *School of Chemistry, University of St. Andrews, Fife KY16 9ST, U.K.*
E-mail: es487@st-andrews.ac.uk; jtsi@st-andrews.ac.uk

1. J. W. Fergus, *Int. J. Hydrogen Energ.*, 2007, **32**, 3664 – 3671.
2. M. Gödickemeier, *Mixed ionic electronic conductors for solid oxide fuel cells*, [Mikrofiche-Ausg.]., 1996.
3. *International Energy Outlook 2011*, U.S. Energy Information Administration, 2011.
4. A. Galich and L. Marz, *Energy, Sustainability and Society*, 2012, **2**, 2.
5. A. Atkinson, S. Barnett, R. J. Gorte, J. T. S. Irvine, A. J. McEvoy, M. Mogensen, S. C. Singhal, and J. Vohs, *Nat. Mater.*, 2004, **3**, 17–27.
6. W. Z. Zhu and S. C. Deevi, *Mat Sci Eng A*, 2003, **362**, 228 – 239.
7. F. H. Stott, F. I. Wei, and C. A. Enahoro, *Materials and Corrosion*, 2004, **40**, 198–205.
8. Horita, K. Yamaji, Y. P. Xiong, H. Kishimoto, N. Sakai, and H. Yokokawa, *Solid State Ionics*, 2004, **175**, 157–163.
9. Fergus, *Int. Mater. Rev.*, 2005, **397**, 271–283.
10. F. Tietz and D. Sebold, *Materials science & engineering. B, Solid-state materials for advanced technology*, **150**, 135–140.
11. L. Cooper, S. Benhaddad, A. Wood, and D. G. Ivey, *J Power Sources*, 2008, **184**, 220–228.
12. Larring and T. Norby, *Journal of the Electrochemical Society*, 2000, **147**, 3251–3256.
13. X. Chen, P. Hou, C. Jacobson, S. Visco, and L. Dejonghe, *Solid State Ionics*, 2005, **176**, 425–433.
14. Z. Yang, G. Xia, X. Li, and J. Stevenson, *International Journal of Hydrogen Energy*, 2007, **32**, 3648–3654.
15. Z. Yang, G.-G. Xia, C.-M. Wang, Z. Nie, J. Templeton, J. W. Stevenson, and P. Singh, *J Power Sources*, 2008, **183**, 660–667.
16. S. C. Singhal, in *Solid Oxide Fuels Cells: Facts and Figures*, eds. J. T. S. Irvine and P. Connor, Springer London, 2013, pp. 1–23.
17. E. Stefan and J. Irvine, *Journal of Materials Science*, 2011, **46**, 7191–7197.
18. S. Tao and J. T. S. Irvine, *Nat. Mater.*, 2003, **2**, 320–323.
19. D. M. Bastidas, S. Tao, and J. T. S. Irvine, *J. Mater. Chem.*, 2006, **16**, 1603–1605.
20. J. C. Ruiz-Morales, J. Canales-Vázquez, J. Peña-Martínez, D. Marrero-López, and P. Núñez, *Electrochim. Acta*, **52**, 278–284.
21. X. Yang and J. T. S. Irvine, *J Mater Chem*, 2008, **18**, 2349–2354.
22. M. Mogensen, N. M. Sammes, and G. A. Tompsett, *Solid State Ionics*, 2000, **129**, 63 – 94.
23. J. H. Kim, D. Miller, H. Schlegl, D. McGrouther, and J. T. S. Irvine, *Chem. Mater.*, 2011, **23**, 3841–3847.
24. G. Kim, G. Corre, J. T. S. Irvine, J. M. Vohs, and R. J. Gorte, *Electrochem. Solid St.*, **11**.
25. M. J. Jørgensen and M. Mogensen, *J. Electrochem. Soc.*, **148**, A433–A442.
26. T. Ramos, J. Hjelm, and M. Mogensen, *J. Electrochem. Soc.*, **158**.
27. I. M. Torres da Silva, J. Nielsen, J. Hjelm, and M. Mogensen, *ECS Transactions*, 2009, **25**, 489–498.
28. C. Xia and M. Liu, *Solid State Ionics*, 2002, **152–153**, 423–430.
29. B. C. H. Steele, *Solid State Ionics*, 2000, **129**, 95–110.
30. S. P. Jiang, L. Zhang, and Y. Zhang, *J. Mater. Chem.*, 2007, **17**, 2627–2635.
31. S. Tao and J. T. S. Irvine, *J. Electrochem. Soc.*, 2004, **151**, A252–A259.
32. M. Gross, J. Vohs, and R. Gorte, *J. Electrochem. Soc.*, 2007, **154**, B694–B699.

